Planning in Information Space for a Quadrotor Helicopter in a GPS-denied Environment

Ruijie He, Sam Prentice and Nicholas Roy

***Abstract*— This paper describes a motion planning algorithm for a quadrotor helicopter flying autonomously without GPS. Without accurate global positioning, the vehicle must use on-board sensors to detect environmental features and infer its position in a pre-existing map. The vehicle's ability to localize itself varies across the environment, since different map features give different degrees of localization information. Therefore, if the vehicle plans a path without regard to how well it can localize itself along that path, it runs the risk of becoming lost.**

We begin by applying the Belief Roadmap (BRM) algorithm [1], an information-theoretic extension of the Probabilistic Roadmap algorithm, to incorporate sensing during the motion planning process in a high-dimensional space. We extend the original BRM to use non-linear state inference via the Unscented Kalman Filter (UKF), and describe a sampling algorithm that minimizes the number of samples required to find a good path. Finally, we demonstrate the BRM path-planning algorithm on the helicopter, navigating in an indoor environment with a laser range-finder.

I. INTRODUCTION

Unmanned air vehicles (UAVs) rely heavily on accurate knowledge of their position for decision-making and control. As a result, considerable investment has been made towards improving the availability of global positioning infrastructure, including utilizing satellite-based GPS system and developing algorithms to leverage existing RF signals such as WiFi. However, important domains, such as indoor environments and the urban canyon, remain without access to external positioning systems. Autonomous UAVs thus currently have limited ability to fly through these areas.

Consequently, there has been considerable growth in the use of environmental sensors for position estimation on mobile robot systems. Vehicle localization using sonar ranging [2], video imaging [3] and laser ranging [4] have been used extremely successfully in a number of applications and have now essentially become commodity technology, especially aboard ground robots. Unfortunately, the UAV community has not been able to leverage these ground vehicle successes for two reasons. First, some of the most successful demonstrations of long-term robot autonomy have used planar laser ranging based on the ubiquitous SICK laser range finder, which normally provides localization information for three dimensions without additional specialized hardware. While this is sufficient for ground vehicle localization, localization in six dimensions during flight requires considerably more data. Second, UAVs are severely constrained by weight and, consequently, power limitations. A vehicle small enough to fly indoors or through populated urban areas safely can carry very little in terms of sensor payload, leading to reduced range and field of view.

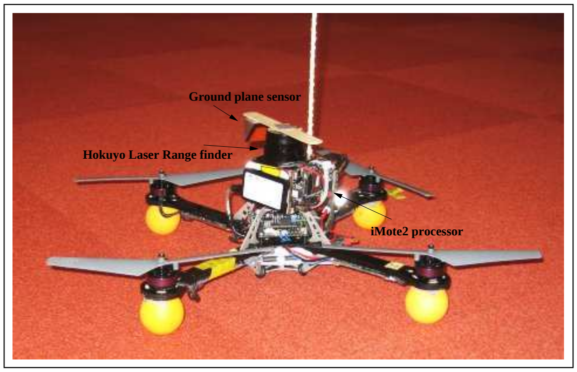

Fig. 1. Our quadrotor helicopter.

Nevertheless, most UAVs can carry *some* sensing capability for localization; they simply cannot carry sensors that enable themselves to localize *everywhere*. If the vehicle can use its sensor model to incorporate predicted measurements into its decision making, then the vehicle can plan trajectories that are robust to sensor limitations. In essence, the planner biases the motion of the vehicle towards paths where the vehicle has high localization capability, trading off the value of fast mission completion against the cost of errors due to poor localization.

In this paper, we describe a planning algorithm for the quadrotor helicopter, shown in Figure 1, and built by Ascent Technology [5]. This vehicle has a laser range-finder capable of estimating position, yaw angle and altitude information from environmental features within a $4m$ range in a $240°$ field of view. The limited range and field of view of the sensor lead to position estimates that vary in accuracy and confidence over the environment.

Our algorithm is based on the Belief Roadmap (BRM) algorithm [1], which is a generalization of the Probabilistic Roadmap (PRM) algorithm [6]. The BRM performs searches in the information space of the vehicle very efficiently by using the sympletic form of the Extended Kalman Filter (EKF) to find the minimum expected cost path for the vehicle. We make two contributions in extending the BRM in this paper. First, while the original formulation of the BRM assumed the Extended Kalman Filter for position tracking, we show how to generalize the BRM to use the Unscented Kalman Filter (UKF) [7] for position tracking, providing better approximation of the non-linearities of UAV motion and laser sensing. Second, the BRM is a sampling-

Ruijie He, Sam Prentice and Nicholas Roy are members of the Computer Science and Artificial Intelligence Laboratory, Massachusetts Institute of Technology, 77 Massachusetts Ave., Cambridge, MA 02139. `ruijie@mit.edu`, `prentice@mit.edu`, `nickroy@mit.edu`

based planner, and the original formulation does not provide guidance in choosing a good sampling function. We use the notion of a "Sensor Uncertainty Field" [8], and show how a model of sensor uncertainty can be used to generate a more efficient representation of the information space. Unlike in previous formulations, we do not need to compute a dense representation of the sensor uncertainty field across the entire configuration space; by sampling from the sensor uncertainty field, we generate a sparse and computationally efficient representation of the localization performance through the environment. Finally, we conclude the paper with a demonstration of the quadrotor helicopter using the BRM algorithm to navigate autonomously indoors.

II. TRAJECTORY PLANNING

We first formulate the problem of motion planning for a UAV. We assume that the vehicle is holonomic and that we have full control authority, allowing us to ignore vehicle dynamics and treat the problem as a kinematic motion planning problem. $\mathcal{C}$ denotes the configuration space [9], the space of all vehicle poses, $\mathcal{C}_{free}$ is the set of all collision-free poses (based on the map $\mathcal{M}$ of obstacle positions) and $\mathcal{C}_{obst}$ is the set of poses resulting in collision with obstacles, so that $\mathcal{C} \equiv \mathcal{C}_{free} \cup \mathcal{C}_{obst}$. Given an initial vehicle state s_0 and a map of the environment, the planning problem is to find a sequence of actions to move the vehicle from state s_0 to a goal state s_g without collisions. Our UAV has 6 degrees of freedom (x, y, z, roll, pitch, yaw), so $\mathcal{C} = \mathcal{R}^6$, which is of moderately high dimension.

One popular algorithm for planning in high dimensional spaces is the Probabilistic Roadmap (PRM) algorithm [6], in which a discrete graph is used to approximate the connectivity of $\mathcal{C}_{free}$. If the graph of $\mathcal{C}_{free}$ contains the start and goal states and a path exists from the start node to the goal node in the graph, then this path also exists in $\mathcal{C}_{free}$. The PRM builds the graph by sampling a set of states randomly from $\mathcal{C}$ (adding the start state s_0 and goal state s_g to the sample set), and then evaluating each state for membership in $\mathcal{C}_{free}$; the assumption is that it is much cheaper to evaluate randomly sampled poses in higher dimensions than it is to build an explicit representation of $\mathcal{C}_{free}$. Samples that lie within $\mathcal{C}_{free}$ constitute the nodes of the PRM graph and edges are placed between nodes where a straight line path between nodes also lies entirely within $\mathcal{C}_{free}$. Given this graph, a feasible, collision-free path can be found using a standard graph search algorithm from the start node to the goal node. The path can be executed by using a simple controller to follow each edge to the goal.

However, the PRM, and its variants, are not yet well-suited to the problem of a GPS-denied UAV, in that executing a plan requires a controller that follows the straight-line edges joining graph points. If the UAV executing the plan does not have a good estimate of its state, it may not be able to determine when it has arrived at a graph node and should start to follow a new edge.

III. VEHICLE POSITION ESTIMATION

If the UAV does not have access to perfect state knowledge, such as through a GPS system, it can still localize itself by using sensors to measure environmental features and then registering those measurements against a pre-existing map. Bayesian statistical analysis is one of the most robust methods of localization, [2], [10], in which a probability distribution $p(s_t|u_{1:t}, z_{1:t})$ over the (unknown) vehicle state s_t at time t is inferred following a series of noisy actions $u_{1:t}$ and measurements $z_{1:t}$. With some standard assumptions about the actions and observations, the posterior belief can be expressed as

$$p(s_t|u_{1:t}, z_{1:t}) = \frac{1}{Z} p(z_t|s_t) \int_S p(s_t|u_t, s_{t-1}) p(s_{t-1}) ds_{t-1}, \quad (1)$$

where Z is a normalization factor. Equation (1), referred to as the Bayes' filter equation, provides an efficient recursion for updating the state distribution. We will refer to $p(s_t) = b_t$ as the vehicle's belief about its position.

There are many different representations of the Bayes' filter equation, but the Kalman filter is one of the most common. The Kalman filter assumes that all probability distributions are Gaussian, and that the transition and observation Gaussians are linearly parameterized by the state and control. The Extended Kalman filter (EKF) allows the same inference algorithm to operate with non-linear transition and observation functions by linearizing these functions around the current mean estimate. More formally, the state s_t and observation z_t are given by the following functions,

$$\begin{aligned} & s_t = g(s_{t-1}, u_t, w_t), \qquad && w_t \sim N(0, W_t), && (2) \\ \text{and} \quad & z_t = h(s_t, q_t), && q_t \sim N(0, Q_t), && (3) \end{aligned}$$

where u_t is a control action, and w_t and q_t are random, unobservable noise variables. The EKF computes the state distribution at time t in two steps: a process step based only on the control input u_t leading to an estimate $p(\overline{s}_t) = N(\overline{\mu}_t, \overline{\Sigma}_t)$, and a measurement step to complete the estimate of $p(s_t)$. The process step follows as

$$\overline{\mu}_t = g(\mu_{t-1}, u_t), \qquad \overline{\Sigma}_t = G_t \Sigma_{t-1} G_t^T + V_t W_t V_t^T, \quad (4)$$

where G_t is the Jacobian of g with respect to s and V_t is the Jacobian of g with respect to w. For convenience, we denote $R_t \triangleq V_t W_t V_t^T$. Similarly, the measurement step follows as:

$$\mu_t = \overline{\mu_t} + K_t(H_t \overline{\mu}_t - z_t), \qquad \Sigma_t = (I - K_t H_t)\overline{\Sigma}_t, \quad (5)$$

where H_t is the Jacobian of h with respect to s and K_t is known as the Kalman gain, given by

$$K_t = \overline{\Sigma}_t H_t^T \left(H_t \overline{\Sigma}_t H_t^T + Q_t \right)^{-1}. \quad (6)$$

An alternate form of the EKF represents the covariance by its inverse, the information matrix [11]. The information matrix updates can be written as

$$\overline{\Omega}_t = \overline{\Sigma}_t^{-1} = \left(G_t \Sigma_{t-1} G_t^T + R_t\right)^{-1} \quad (7)$$

$$\Omega_t = \overline{\Omega}_t + H_t^T Q_t^{-1} H_t. \quad (8)$$

For convenience, we denote $M_t \triangleq H_t^T Q_t^{-1} H_t$ such that $\Omega_t = \overline{\Omega}_t + M_t$. The distribution $p(s_t|u_{1:t}, z_{1:t})$ can be represented by the information vector ξ_t and the information matrix $\Omega_t = \Sigma_t^{-1}$ and may be more efficient to compute in domains where the information matrix is sparse.

IV. BELIEF SPACE PLANNING

Recall from section II that the PRM planning algorithm constructs a graph in the state space $\mathcal{C}_{free}$ of the vehicle. However, the vehicle does not know its actual state but only has access to the EKF state estimate $b = (\mu, \Sigma)$; by planning in the *belief space* (or information space), the vehicle can distinguish between state estimates where the norm of the covariance is small (i.e., the vehicle has high confidence in its mean state estimate) and state estimates where the norm of the covariance is large (i.e., the mean state estimate is uncertain). Ideally, beliefs with high uncertainty are to be avoided, and if encountered, conservative sensing action would be a reasonable response.

Conventional motion planners generally search for a collision-free path that minimizes the distance to the goal location. In belief space, every belief typically has some probability that the robot is at the goal state. A more appropriate objective function is therefore to maximize the probability of the goal state, and extensions of the PRM to optimization (as opposed to satisficing, searching for a feasible plan) have been explored elsewhere [12], [13].

A naive approach to planning in belief space would therefore involve sampling beliefs directly from (μ, Σ), adding the initial belief b_0 to construct the graph nodes, placing edges between pairs of beliefs (b^i, b^j) for which a controller exists that can take the vehicle from belief b^i to b^j, and then carrying out graph search as before. Unfortunately, it has been shown [1] that the likelihood is zero of sampling any beliefs that are actually reachable from the initial belief b_0.

However, the EKF representation of the belief space carries an extremely useful property. Each belief b_t is a factored combination of μ and Σ. Under some mild assumptions of unbiased motion and sensor models, the reachability of any μ is a function of the vehicle kinematics and the environmental structure as in the PRM. For some μ that is reachable along a path from μ_0, the corresponding reachable covariance can be predicted by propagating the initial covariance Σ_0 along the path using equations (4) and (5) and the motion and sensing models.

Therefore, to construct a graph of the reachable belief space, the planner first samples a set of mean poses $\{\mu_i\}$ from $\mathcal{C}_{free}$ using the standard pose sampling of the PRM algorithm, and places an edge e_{ij} between pairs (μ_i, μ_j) if the straight line between poses is collision-free. Forward search is used to search for a path through the graph, but each step of the search computes the posterior covariance at each node instead of the standard cost-to-go.

A. Belief Updating as a One-Step Operation

The most computationally demanding aspect of the graph-search algorithm described above is in propagating the initial covariance Σ_0 to each graph node. Covariance propagation requires multiple EKF updates along each edge e_{ij}, and while this operation is a constant multiplier of the asymptotic search complexity, it can still dominate the overall search time. Furthermore, these EKF updates are not a one-time cost; the search process will find multiple paths to node i. Each of these paths will lead to a different posterior covariance at node i, and each such covariance must be propagated along edge e_{ij} to reach node j, incurring the computational cost of propagating along the edge (some series of EKF updates) for each covariance. The BRM algorithm avoids this complexity by using an alternate representation of the covariance that allows multiple EKF updates to be compiled into single linear transfer function. By pre-computing the transfer function for each edge, the search complexity for belief space planning becomes comparable to configuration space planning.

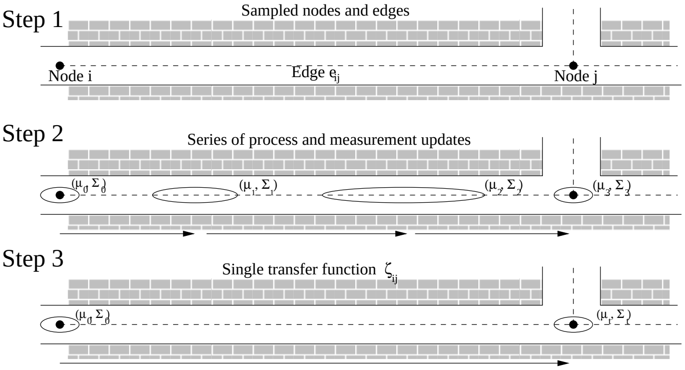

Fig. 2. The Belief Roadmap with one-step transfer functions calculated using the UKF. In step 1, the graph of mean poses is constructed, and mutually visible nodes are connected with edges. In step 2, the posterior covariance is calculated through a series of process and measurement updates. In step 3, the one-step covariance transfer function is calculated from the individual multi-step updates.

It has been shown previously [14], [1] that the covariance of a Kalman filter-based state estimator can be factored as $\Sigma = BC^{-1}$, where the combined process and measurement update for an EKF gives B_t and C_t as linear functions of B_{t-1} and C_{t-1}.

$$\text{Given: } \Sigma_{t-1} = B_{t-1}C_{t-1}^{-1} \tag{9}$$

$$\Rightarrow \overline{\Sigma}_t = G_t B_{t-1} C_{t-1}^{-1} G_t^T + R_t \tag{10}$$

$$= (G_t B_{t-1})(G_t^{-T} C_{t-1})^{-1} + R_t \tag{11}$$

$$= \left(\overline{D}_t \overline{E}_t^{-1}\right)^{-1} \tag{12}$$

where $\overline{D}_t = G_t^{-T} C_{t-1}$ and $\overline{E}_t = G_t B_{t-1} + R_t(G_t^{-T} C_{t-1})$ and equation (12) follows from a matrix inversion lemma. The covariance update in the information form can similarly be factored as

$$\Sigma_t = (\overline{\Sigma}_t^{-1} + H_t^T Q_t^{-1} H_t^T)^{-1} \tag{13}$$

$$= (\overline{D}_t \overline{E}_t^{-1} + M_t)^{-1} \tag{14}$$

Using the same matrix inversion lemma,

$$= \overline{E}_t(\overline{D}_t + M_t \overline{E}_t)^{-1} \tag{15}$$

$$\Rightarrow \Sigma_t = B_t C_t^{-1}, \tag{16}$$

where $B_t = \overline{E}_t = G_t B_{t-1} + R_t(G_t^{-T} C_{t-1})$ and $C_t = (\overline{D}_t + M_t \overline{E}_t) = G_t^{-T} C_{t-1} + M_t G_t B_{t-1} + R_t(G_t^{-T} C_{t-1})$. In both cases, B_t and C_t are linear functions of B_{t-1} and C_{t-1}. Collecting terms, we can write the complete update step linearly, such that

$$\Psi_t = \begin{bmatrix} B \\ C \end{bmatrix}_t = \begin{bmatrix} 0 & I \\ I & M \end{bmatrix}_t \begin{bmatrix} 0 & G^{-T} \\ G & RG^{-T} \end{bmatrix}_t \begin{bmatrix} B \\ C \end{bmatrix}_{t-1}, \tag{17}$$

Algorithm 1 The Belief Roadmap (BRM) algorithm.

```
Require: Start belief $(\mu_0, \Sigma_0)$, goal $\mu_{goal}$ and map $\mathcal{C}$
 1: Sample poses $\{\mu_i\}$ from $\mathcal{C}_{free}$ to build belief graph node
    set $\{n_i\}$ such that $n_i = \{\mu = \mu_i, \Sigma = \emptyset\}$
 2: Create edge set $\{e_{ij}\}$ between nodes $(n_i, n_j)$ if the
    straight-line path between $(n_i[\mu], n_j[\mu])$ is collision-free
 3: Build one-step transfer functions $\{\zeta_{ij}\} \quad \forall \quad e_{ij} \in \{e_{ij}\}$
 4: Augment node structure with best path $p=\emptyset$, such that
    $n_i=\{\mu, \Sigma, p\}$
 5: Create search queue with initial position and covariance
    $Q \leftarrow n_0 = \{\mu_0, \Sigma_0, \emptyset\}$
 6: while $Q$ is not empty do
 7:   Pop $n \leftarrow Q$
 8:   if $n = n_{goal}$ then
 9:     Continue
10:   end if
11:   for all $n'$ such that $\exists e_{n,n'}$ and not $n' \ni n[p]$ do
12:     Compute one-step update $\Psi' = \zeta_{n,n'} \cdot \Psi$, where
        $\Psi = \begin{bmatrix} n[\Sigma] \\ I \end{bmatrix}$
13:     $\Sigma' \leftarrow \Psi'_{11} \cdot {\Psi'_{21}}^{-1}$
14:     if $tr(\Sigma') < tr(n'[\Sigma])$ then
15:       $n' \leftarrow \{n'[\mu], \Sigma', n[p] \cup \{n'\}\}$
16:       Push $n' \rightarrow Q$
17:     end if
18:   end for
19: end while
20: return $n_{goal}[p]$
```

where Ψ_t is the stacked block matrix $\begin{bmatrix} B \\ C \end{bmatrix}_t$ consisting of the covariance factors and $\zeta_t = \begin{bmatrix} W & X \\ Y & Z \end{bmatrix}_t$ is the one-step transfer function for the covariance factors for G_t, H_t, R_t and M_t.

Notice that all of the elements in ζ are directly controllable, except for M_t, which is related to the measurement z_t but is not a function of the measurement itself. M_t represents the total amount of information that the measurement provides at time t and depends on the measurement noise model Q (which is usually constant) and the measurement Jacobian H_t. The accuracy of the EKF approximation assumes that the measurement function is locally linear, which is exactly the approximation that the Jacobian is locally constant. As a result, whenever the EKF assumptions hold, then we can assume that M_t is constant and known *a priori*. This allows us to determine ζ_t for any point along a trajectory; furthermore, the linearity of the update allows us to combine multiple ζ_t matrices into a single, one-step update for the covariance along the entire length of a trajectory. Therefore, for each edge e_{ij} in the BRM graph, we can pre-compute each ζ_t along the edge from the relevant Jacobians and then multiply the set of ζ_t's into a single transfer function ζ_{ij} that will propagate an initial (factored) covariance along the length of the edge in a single matrix multiply. Figure 2 shows this process of constructing the transfer function for each edge.

Table 1 describes the complete Belief Roadmap algorithm. Step 2 of the algorithm contains a pre-processing phase where each edge is labeled with the transfer function ζ_{ij} that allows each covariance to be propagated in a single step.

V. THE UNSCENTED KALMAN FILTER

The critical step of the BRM algorithm is the construction of the transfer function, which depends on terms R_t and M_t, the projections of the process and measurement noise terms into the state space. R_t and M_t also represent the information lost due to motion, and the information gained due to measurements. When using the Extended Kalman filter to perform state estimation, these terms are trivial to compute. However, the EKF is not always a feasible form of Bayesian filtering, especially when linearizing the control or measurement functions leads to a poor approximation. A particularly relevant application where EKF state estimation fares poorly is localization in discrete or grid-based maps. Grid map representations contain a strong independence assumption between the grid cells, which causes measurements of neighboring grid cells to appear uncorrelated. When computing the Jacobian of a measurement with respect to a grid cell, however, the gradient of the measurement is strongly correlated with the neighboring cells. As a result, EKF localization requires high-level features such as walls and corners to be extracted for use in both computing the innovation of the measurements and computing the Jacobians. This example is one of a number of problems that can occur with a standard EKF implementation.

In order to address the limitations of linearization, alternate forms of the Bayes filter have been developed. One recent extension is the Unscented Kalman filter (UKF) [7], which uses a set of $2n + 1$ deterministic samples, known as "sigma points" from an assumed Gaussian density to represent the probability density of a space of dimensionality n. These samples are generated according to:

$$\mathcal{X}_t^0 = \mu_{t-1}, \tag{18}$$

$$\mathcal{X}_t^i = \mu_{t-1} + \left(\sqrt{(n+\lambda)\Sigma_t}\right)^i, \quad i=1,\ldots,n \tag{19}$$

$$\mathcal{X}_t^i = \mu_{t-1} - \left(\sqrt{(n+\lambda)\Sigma_t}\right)^i, \quad i=n+1,\ldots,2n \tag{20}$$

where $\left(\sqrt{(n+\lambda)\Sigma_t}\right)^i$ is the ith column of the root of the matrix. Each sigma point $\mathcal{X}^i$ has an associated weight w_m^i used when computing the mean, and w_c^i is the weight used when computing the covariance, such that $\sum_{i=0}^{2n} w_c^i = 1$, $\sum_{i=0}^{2n} w_m^i = 1$. The weights and the λ parameters model the width of the covariance; the mechanism for choosing these parameters can be found in [7]. The samples are propagated according to the non-linear process model such that

$$\overline{\mathcal{X}}_t^i = g(\mathcal{X}_t^i, u, 0), \tag{21}$$

generating the process mean and covariance

$$\overline{\mu}_t = \sum_{i=0}^{2n} w_m^i \overline{\mathcal{X}}_t^i \tag{22}$$

$$\overline{\Sigma}_t = \sum_{i=0}^{2n} w_c^i (\overline{\mathcal{X}}_t^i - \overline{\mu}_t)(\overline{\mathcal{X}}_t^i - \overline{\mu}_t) + R_t. \tag{23}$$

The sigma points are used to create sigma points in the measurement space, which are then transformed to generate the posterior mean and covariance (μ_t, Σ_t), such that

$$\overline{\mathcal{Z}}_t^i = h(\overline{\mathcal{X}}_t^i, 0) \qquad \overline{\mu}_t^z = \sum_{i=0}^{2n} w_m^i \overline{\mathcal{Z}}_t^i \tag{24}$$

$$S_t = \left(\sum_{i=0}^{2n} w_m^i (\overline{\mathcal{Z}}_t^i - \overline{\mu}_t^z)(\overline{\mathcal{Z}}_t^i - \overline{\mu}_t^z) \right) + Q_t \tag{25}$$

$$K_t = \left(\sum_{i=0}^{2n} w_c^i (\overline{\mathcal{X}}_t^i - \overline{\mu}_t)(\overline{\mathcal{Z}}_t^i - \overline{\mu}_t^z) \right) S_t^{-1} \tag{26}$$

$$\mu_t = \overline{\mu}_t + K_t(z_t - \overline{\mu}_t^z) \tag{27}$$

$$\Sigma_t = \overline{\Sigma}_t - K_t S_t K_t. \tag{28}$$

The advantage to the UKF formulation is that the process and measurement functions are not projected into the state space by a linearization; instead, the Unscented Transform computes the moments of the process and measurement distributions directly in the state space itself. As a result, the UKF eliminates the need for linearization and captures the distribution accurately up to the second order, rather than just the first order fidelity of the EKF.

Unfortunately, although the UKF provides a mechanism of efficiently tracking the posterior distribution as a Gaussian while avoiding linearization of the measurement model, the UKF no longer calculates the M_t matrix which is a critical piece of the individual transfer functions ζ_t. However, we can still recover M_t from the UKF update directly by working in the information form and noticing that M_t is the information gain due to measurement z_t. We can therefore combine equation (8) and equation (28),

$$\Omega_t = \overline{\Omega}_t + M_t \tag{29}$$

$$\Rightarrow M_t = \Omega_t - \overline{\Omega}_t \tag{30}$$

$$= \Sigma_t^{-1} - \overline{\Sigma}_t^{-1} \tag{31}$$

$$= (\overline{\Sigma}_t - K_t S_t K_t)^{-1} - \overline{\Sigma}_t^{-1} \tag{32}$$

In order to calculate the M matrix for a series of points along a trajectory, we can generate a prior covariance and compute the posterior covariance as in equation (28). Happily, the UKF covariance update does not depend on the actual measurement received, exactly like the EKF covariance update.

The UKF is still a projection of the measurement noise into the state space, but is a more accurate projection than an explicit linearization of the measurement model. By representing the belief update process with the one-step transfer function, we are approximating the non-linear UKF update. Figure 3(a) depicts the difference between covariances computed using the full UKF update and covariances computed using the one-step transfer function for a range of motions and randomized initial conditions. As expected, the one-step transfer function using the M matrix calculated in equation (32) is an approximation to the UKF model but the induced error is low; the trace of the covariances are closely matched.

The UKF calculation of the information gain M_t *does*, however, depend on the specific prior matrix $\overline{\Sigma}_t$. As a result, different choices of prior for equation (32) may result in different one-step transfer functions. Figure 3(b) shows a distribution of the ratio of the error of the one-step covariance to the full UKF covariance, where 7000 trials were performed using 100 different priors and a range of initial conditions and trajectories were used to calculate the M matrix. The error induced in the one-step transfer function for using a constant M is less than 2% with a significance of $p = 0.955$, indicating low sensitivity to the choice of prior over a range of operating conditions.

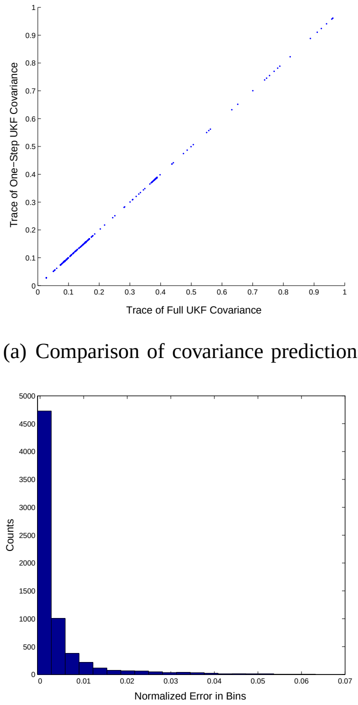

(a) Comparison of covariance predictions

(b) Distribution of error using constant prior approximation

Fig. 3. (a) Comparison of trace of covariance from full UKF filtering and trace of covariance from one-step transfer function using UKF M matrix. (b) Distribution of ratio of error induced by computing the M matrix for the one-step transfer function using a constant prior.

VI. Sampling in Belief Space

As the number of samples and the density of the graph grows, the BRM planning process will find increasingly low-covariances paths. However, as the density of the graph grows, the cost of searching the graph will also grow; searching the graph will have complexity $\mathcal{O}(b^d)$ for b edges per node and path of length d edges. We can reduce this complexity by minimizing the size of the graph, sampling nodes that reflect the useful part of the information space.

The optimal sampling strategy would generate samples that lie only on the optimal path to the goal; this would of course require knowing the optimal path beforehand. However, some samples are more likely to be useful than others: vehicle poses that generate measurements with high information value are much more likely to lie on the optimal path than vehicle poses that generate measurements with little information. If poses are initially sampled from $\mathcal{C}$ uniformly, but are retained according to the expected information gain from sensing at each point, the graph will converge to one that maintains the connectivity of the

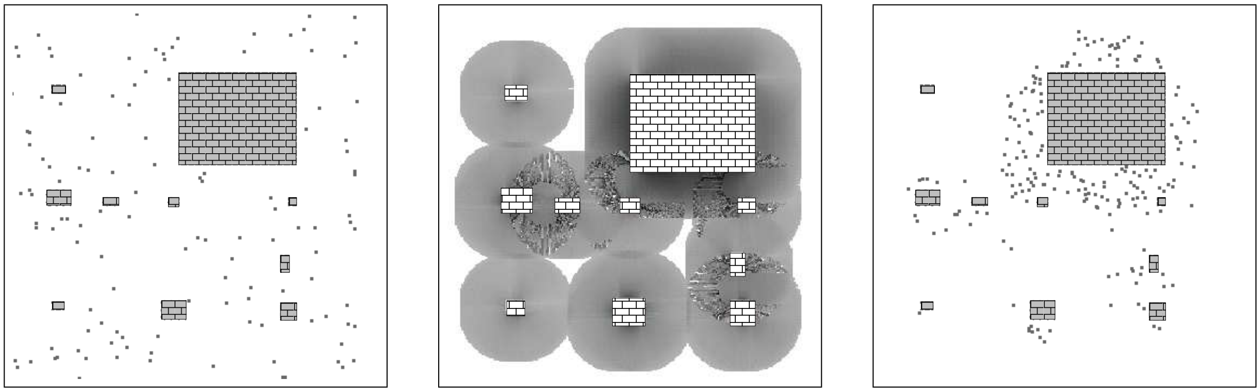

(a) Samples drawn uniformly

(b) Sample map of sensor uncertainty field

(c) Samples from sensor uncertainty field

Fig. 4. Bird's-eye view of unstructured, GPS-denied environment. The brick structures are pillars in the underground garage. (a) Distribution of samples drawn uniformly. (b) The sample map with the sensor uncertainty field. The intensity (darkness) of each pixel corresponds to the information gain available by sensing there. (c) Distribution of samples drawn according to the sensor uncertainty field.

free space and places nodes that maximize the localization accuracy of the vehicle. We call this sampling strategy *sensor uncertainty* sampling, after the "Sensor Uncertainty Field" (SUF) defined by Takeda and Latombe [8]. By sampling from this field in building the BRM graph, we gain the benefits of focusing the search on the states that lead to high information gain without the cost of explicitly building the sensor uncertainty field.

Information gain is calculated from the difference in entropy of the prior and posterior distributions,

$$\mathcal{I}(x) = H(p(x|z)) - H(p(x)) \tag{33}$$

where entropy is

$$H(p(x)) = -\int p(x) \log p(x). \tag{34}$$

In practice, we use a constant prior $p(x) = \Sigma_0$ such that $H(p(x)) = C$ and Bayes' rule to compute $p(x|z) = p(z|x) \cdot p(x)$, such that

$$\mathcal{I}(x) = H(p(x|z)) - C \tag{35}$$

where $z = \operatorname{argmax}_z p(z|x)$ and $p(x|z)$ is calculated according to the UKF. We normalize the posterior entropies so that $\mathcal{I}(x)$ lies in the range $[0, 1]$, allowing us to treat the information gain of x as a probability that the sample is accepted or rejected.

Figure 4(a) shows a bird's-eye view of an example environment with limited structure and no GPS, specifically, the Stata Center parking garage at MIT. The brick structures in figures 4(a) and (c) are the parking garage pillars and stairwell (top right). In figure 4(a), sample poses are drawn uniformly. Figure 4(b) shows the sensor uncertainty field [8] where equation (33) is evaluated at each location (x, y) for fixed height and attitude. (The lack of smoothness between obstacles is an artifact of the rendering process and angular discretization.) The pixel intensity corresponds to the information gain, where darker pixels have more information. This field is shown only to illustrate the concept; computing the field for realistic domains is impractical. Finally, figure 4(c) shows samples drawn according to the sensor uncertainty. Note that the sample density is lowest far from the environmental structure where sensing provides the least amount of information.

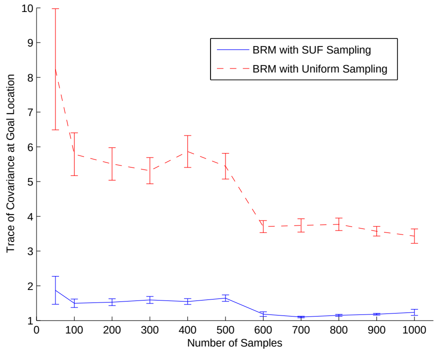

Fig. 5. Comparison of uniform vs. sensor uncertainty sampling strategies. The sensor uncertainty sampler finds accurate trajectories with considerably fewer samples than the uniform sampler.

Figure 5 shows the advantage of sampling according to the sensor uncertainty. The graph constructed using sensor uncertainty sampling consistently found a trajectory resulting in a covariance with trace 1.48 using 100 samples, whereas the uniform sampling method required 1000 samples to achieve a covariance of size 3.43. By sampling uniformly, the standard BRM requires a large and dense graph to achieve good localization accuracy. Table I shows a comparison of graph construction and planning times. The conventional PRM is clearly the fastest algorithm in both graph construction speed and path search, but the localization performance is expectedly poor. The BRM with sensor uncertainty sampling requires additional time during the graph creation phase, but this time can be amortized across multiple queries, and results in measurably better paths.

	Trace Goal Covariance	Graph Build Time (s)	Path Search Time (s)
PRM	16.046	0.036	0.001
BRM, Uniform Sampling	4.223	18.920	0.039
BRM, Sensor Uncertainty Sampling	1.094	25.589	0.032

TABLE I

PERFORMANCE AND TIME COSTS OF DIFFERENT PLANNERS.

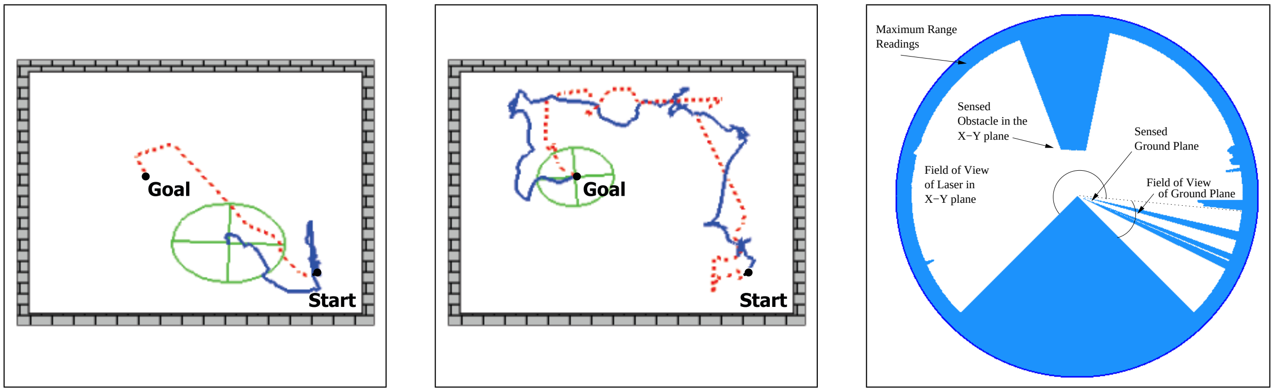
Goal
Start
Goal
Start
Maximum Range Readings
Sensed Obstacle in the X−Y plane
Sensed Ground Plane
Field of View of Laser in X−Y plane
Field of View of Ground Plane

(a) PRM trajectory, uniform sampling

(b) BRM trajectory, SU sampling

(c) Laser Perception Model

Fig. 6. (a) and (b) show an example indoor environment for comparing the performance of the BRM algorithm. The dashed line is the trajectory computed by the respective algorithms, and the solid line is the localization estimate of the helicopter's position during the execution of the planned trajectory. The ellipse denotes the uncertainty of the helicopter when it reaches the end goal. (a) The trajectory planned by the PRM and the localization estimate of the trajectory flown by the helicopter. (b) The trajectory planned by the BRM using sensor uncertainty sampling and the localization estimate of the trajectory flown by the helicopter. (c) The perception model of the onboard laser range-finder, including the field of view of the X-Y plane and the field of view of the ground plane.

VII. INDOOR NAVIGATION RESULTS

The BRM algorithm and sensor-maximizing sampling strategy were tested using the quadrotor helicopter, shown in Figure 1. Equipped with auto-stabilization rate gyros and accelerometers, the helicopter has on-board attitude control and thus acts as a stable sensor platform. The on-board environmental sensor is a Hokuyo URG laser sensor – a planar laser rangefinder that provides a 240° field-of-view at 10 Hz, up to an effective range of 3m. The laser is mounted in the X-Y plane of the helicopter, and we modified the laser to optically redirect 20° of its field-of-view to provide a small set of range measurements in the (downward) z direction. In a single scan, the vehicle is therefore able to estimate its position, yaw orientation and altitude with respect to environmental features. Figure 6(c) shows an example scan. In practice, the measurement of the ground plane is relatively noisy, although sufficient for closed-loop altitude control.

In this task, the helicopter is required to plan a path to traverse from the starting position to the end goal, shown in Figures 6(a-b), and must constantly be able to localize itself while executing the planned trajectory. To compare the performance of the BRM algorithm using the sensor uncertainty sampling strategy, as opposed to a traditional PRM algorithm performing uniform sampling, we first plan a path for the helicopter using each method. We then manually fly the helicopter through the environment using the planned trajectories, recording both the helicopter's laser range measurements and the motion commands that were transmitted to the helicopter. The sensor and control data were then used to test the localization ability of the helicopter when executing the given planned trajectory.

Figure 6(a) shows an example trajectory generated by the traditional PRM planner, which finds a direct path from start to goal. Because this plan ignores the helicopter's need for sensor information to localize itself, the helicopter is highly uncertain of its position by the end of the executed trajectory, and suffers a localization error of 259cm at the goal. On the other hand, an example BRM trajectory using sensor uncertainty sampling enables the helicopter to stay well-localized, as shown in Figure 6(b). The helicopter achieves this by detouring from the shortest path toward areas of high sensor information, resulting in an error at the goal of only 9cm, as well as low uncertainty in its final position, as shown by the size of the ellipse in Figure 6(b). This demonstrates that the BRM trajectory leads to measurably more accurate performance.

VIII. RELATED WORK

Modern approaches to planning with incomplete state information are typically based on the partially observable Markov decision process (POMDP) model [15] or cast as a graph search through belief space [16]. Computing POMDP solutions requires finding an optimal action for each possible belief in the entire belief space. While the POMDP provides a general framework for belief space planning, as the size of the belief space grows POMDP techniques become computationally intractable. The complexity of the solution grows exponentially in both the number of possible control outcomes and the number of potential observations. Numerous approximation algorithms continue to mitigate the problem of scalability [17], [18], but to date POMDP techniques still face computational issues in addressing large problems.

The concept of the information gain at each location is related to the Sensor Uncertainty Field (SUF) [8], which estimates the distribution of possible errors in robot configuration that may result from sensing at each location in space. At every position in the map, the SUF is an estimate of the expected localization error when the robot's sensor data at state x is matched against a prior environment model. A pre-computed SUF model therefore provides the path-planner with a method for selecting safer paths by tracing those points that result in less positional uncertainty. Alternatively, the Augmented MDP uses the concept of information gain by the sensor at each possible pose in the environment freespace [19] in order to compute a dense policy. The

Augmented MDP approach is strongly related to the ideas in this paper, but does not scale well to more than two dimensions.

The extended Kalman filter and unscented Kalman filter have been used extensively. Ko et al. [20] use the iMote2 technology and the UKF for state estimation in aerial vehicles, and Valenti et al. [21] were the first to demonstrate reliable navigation and position estimation on quadrotor helicopters. The sympletic form (and related Hamiltonian form) of the covariance update has been reported before, originally in [22]. Most recently, Mourikis et al. [23] used a semi-definite programming approximation to optimize the Riccati equation corresponding to the covariance update for a set of sensors, solving the problem of optimal measurement frequencies as a convex optimization problem. Finally, laser range finding on-board helicopters is not a novel technology [24], [25], although we believe we are the first to demonstrate reliable autonomous localization and motion planning on an indoor helicopter using laser range finding.

IX. CONCLUSION

In this paper, we have addressed the problem of a helicopter localizing and navigating in GPS-denied environments. The helicopter uses laser range data and an existing map to localize, but the laser has a limited field of view, causing the helicopter to lose track of its own position in certain configurations and in some parts of the environment. We showed how the Belief Roadmap algorithm [1] can be used to plan trajectories through the environment that incorporate a predictive model of sensing, allowing the planner to minimize the positional error of the helicopter at the goal using efficient graph search. The original BRM algorithm assumed an extended Kalman filter model for position estimation, and we showed how this algorithm can be extended to use the unscented Kalman filter. Furthermore, we showed that by choosing an appropriate sampling algorithm, the BRM can find better trajectories with fewer samples than using uniform sampling strategies.

X. ACKNOWLEDGEMENTS

Ruijie He was supported by the government of Singapore, and Sam Prentice and Nicholas Roy were supported by Draper Laboratories under URPP “Robust Distributed Sensor Networks”. This project was supported by the Office of the Dean, School of Engineering and the MIT Air Vehicle Research Center (MAVRC). Jan Stumpf and Daniel Gurdan provided the quadrotor helicopter and the support of Ascending Technologies. Col. Peter Young, Jonathan How, Spencer Ahrens and Brett Bethke provided additional support in the development of the vehicle. Dirk Hähnel, Karl Koscher, Jonathan Lester and Adam Rea provided considerable assistance with the iMote2 package including the MSB and LSB boards. Finally, Intel Labs Seattle and University of Washington donated the iMote hardware. The authors wish to thank this large group of people in support of this project.

REFERENCES

[1] S. Prentice and N. Roy, “The belief roadmap: Efficient planning in linear pomdps by factoring the covariance,” in *Proceedings of the International Symposium on Robotics Research*, 2007.

[2] J. Leonard and H. Durrant-Whyte, “Mobile robot localization by tracking geometric beacons,” *IEEE Transactions on Robotics and Automation*, vol. 7, no. 3, pp. 376–382, June 1991.

[3] R. Sim and G. Dudek, “Comparing image-based localization methods,” in *Proceedings of the Eighteenth International Joint Conference on Artificial Intelligence (IJCAI)*, Acapulco, Mexico, 2003.

[4] S. Thrun, D. Fox, W. Burgard, and F. Dellaert, “Robust monte carlo localization for mobile robots,” *Artificial Intelligence*, vol. 128, no. 1-2, pp. 99–141, 2000.

[5] D. Gurdan, J. Stumpf, M. Achtelik, K. Doth, G. Hirzinger, and D. Rus, “Energy-efficient autonomous four-rotor flying robot controlled at 1 khz,” in *Proc. ICRA*, 2007.

[6] L. E. Kavraki, P. Svestka, J.-C. Latombe, and M. Overmars, “Probabilistic roadmaps for path planning in high dimensional configuration spaces,” *IEEE Transactions on Robotics and Automation*, vol. 12, no. 4, pp. 566–580, 1996.

[7] S. Julier, J. Uhlmann, and H. Durrant-Whyte, “A new approach for filtering nonlinear systems,” in *Proceedings of the American Control Conference*, 1995, pp. 1628–1632.

[8] H. Takeda and J. Latombe, “Sensory uncertainty field for mobile robot navigation,” *Robotics and Automation, 1992. Proceedings., 1992 IEEE International Conference on*, pp. 2465–2472, 1992.

[9] T. Lozano-Perez., “Spatial planning: A configuration space approach,” *IEEE Transactions on Computers*, vol. C-32, no. 2, pp. 108–120, February 1983.

[10] D. Fox, W. Burgard, and S. Thrun, “Active Markov localization for mobile robots,” *Robotics and Autonomous Systems*, vol. 25, no. 3-4, pp. 195–207, 1998.

[11] S. Thrun, Y. Liu, D. Koller, A. Y. Ng, Z. Ghahramani, and H. Durrant-Whyte, “Simultaneous Localization and Mapping with Sparse Extended Information Filters,” *The International Journal of Robotics Research*, vol. 23, no. 7-8, pp. 693–716, 2004.

[12] L. K. Dale, “Optimization techniques for probabilistic roadmaps,” Ph.D. dissertation, Department of Computer Science, Texas A & M University, December 2000.

[13] B. Burns and O. Brock, “Toward optimal configuration space sampling,” in *Proceedings of Robotics: Science and Systems*, Cambridge, MA, 2005.

[14] D. Vaughan, “A nonrecursive algebraic solution for the discrete Riccati equation,” *Automatic Control, IEEE Transactions on*, vol. 15, no. 5, pp. 597–599, 1970.

[15] E. Sondik, “The Optimal Control of Partially Observable Markov Processes,” Ph.D. dissertation, Stanford, 1971.

[16] B. Bonet and H. Geffner, “Planning with incomplete information as heuristic search in belief space,” *Proc. AIPS*, pp. 52–61, 2000.

[17] J. Pineau, G. Gordon, and S. Thrun, “Point-based value iteration: An anytime algorithm for POMDPs,” *International Joint Conference on Artificial Intelligence (IJCAI)*, vol. 13, 2003.

[18] T. Smith and R. Simmons, “Heuristic search value iteration for POMDPs,” *Proceedings of the 20th conference on Uncertainty in artificial intelligence*, pp. 520–527, 2004.

[19] N. Roy and S. Thrun, “Coastal navigation with mobile robots,” in *Advances in Neural Processing Systems 12*, vol. 12, 1999.

[20] J. Ko, D. Klein, D. Fox, and D. Hähnel, “GP-UKF: unscented kalman filters with gaussian process prediction and observation models,” in *Proceedings of the IEEE/RSJ International Conference on Inteligent Robots and Systems (IROS)*, 2007.

[21] M. Valenti, B. Bethke, G. Fiore, J. P. How, and E. Feron, “Indoor multi-vehicle flight testbed for fault detection, isolation, and recovery,” in *Proceedings of the AIAA Guidance, Navigation and Control Conference*, 2006.

[22] J. E. Potter and W. E. van der Velde, “Optimum mixing of gyroscope. and star tracker data,” *Jour. Spacecraft and Rockets*, vol. 5, no. 5, 1968.

[23] A. Mourikis and S. Roumeliotis, “Optimal sensor scheduling for resource constrained localization of mobile robot formations,” *IEEE Transactions on Robotics*, vol. 22, no. 5, pp. 917–931, October 2006.

[24] S. Thrun, M. Diel, and D. Hähnel, “Scan alignment and 3d surface modeling with a helicopter platform,” in *Proceedings of the International Conference on Field and Service Robotics*, 2003.

[25] L. O. Mejias, S. Saripalli, P. Cervera, and G. S. Sukhatme, “Visual servoing of an autonomous helicopter in urban areas using feature tracking,” *Journal of Field Robotics*, vol. 23, no. 3, pp. 185–199, 2006.